JOURNAL OF SPACECRAFT AND ROCKETS
Vol. 44, No. 1, January–February 2007

Survey of Ballute Technology for Aerocapture

Reuben R. Rohrschneider* and Robert D. Braun†
Georgia Institute of Technology, Atlanta, Georgia 30332-0150

DOI: 10.2514/1.19288

NOMENCLATURE

A = projected frontal area, m^2
C_D = drag coefficient
C_L = lift coefficient
C_m = pitching moment coefficient
d = payload base diameter, m
F = axial load on membrane at the center of the aft end of the ballute, N
k = meridian cord factor, $nT_m/P_{\text{rb}}\pi r_b^2$
L/D = lift to drag ratio
L_0 = rigid vehicle length, m
l = tow line length, m
M = vehicle mass, kg
n = number of gores, number of meridian cords
P = circumferential force in torus due to radial load, N
P_{rb} = pressure difference on membrane at maximum ballute diameter, Pa
p = ballute fill pressure, Pa
q = dynamic pressure, $0.5\rho V^2$, Pa
q_w = heat rate, W/cm^2
R = major radius of torus, m
r = minor radius of torus, m
r_b = base radius of vehicle, m
Re = Reynolds number
St = Stanton number
S_0 = unstretched length of ballute membrane, m
T_m = tension in each meridian cord, N
V = velocity, m/s
x = fill pressure to elasticity ratio, m^3/kg
α = angle of attack, deg
β = ballistic coefficient, M/C_DA, kg/m^2
γ = ratio of specific heats
Δ = overpressure parameter
ρ = density, kg/m^3
σ = axial load factor, $F/P_{\text{rb}}\pi r_b^2$
φ = membrane elastic constant, N/m

I. INTRODUCTION

THE concept of using aerodynamic lift and drag to effect a change in orbital energy or plane is classified as aeroassist. First introduced in 1960, aeroassist techniques were shown to have substantial mass savings over propulsive methods in [1,2]. Many types of aeroassist trajectories exist including direct entry, entry from orbit, aerocapture, aerobraking, and aerogravity assist. This paper's focus is aerocapture.

In an aerocapture maneuver, aerodynamic forces are used to decelerate a vehicle from its hyperbolic approach trajectory into a closed orbit about a planet in a single atmospheric pass. The mission profile is illustrated in Fig. 1 and shows the small propulsive periapsis raise maneuver required to achieve orbit. The velocity increment removed during the atmospheric pass can be controlled by modulating the vehicle's aerodynamic lift (using either angle-of-attack or bank angle control) or changing the vehicle drag during the atmospheric pass. Aerocapture subjects an orbiter to much higher

Reuben R. Rohrschneider received his B.S. in aerospace engineering from the University of Michigan and his M.S. in aerospace engineering from the Georgia Institute of Technology. He is currently pursuing his Ph.D. as a graduate research assistant in the Space Systems Design Laboratory in the Guggenheim School of Aerospace Engineering at the Georgia Institute of Technology. His research has included hypersonic aeroelasticity, space systems design and optimization, and planetary entry and aerocapture.

Robert D. Braun is the David and Andrew Lewis Associate Professor of Space Technology in the Guggenheim School of Aerospace Engineering at the Georgia Institute of Technology. As director of Georgia Tech's Space Systems Design Laboratory, he leads a research program focused on the design of advanced flight systems and technologies for planetary exploration. He is responsible for undergraduate and graduate level instruction in the areas of space systems design, astrodynamics, and planetary entry. Before coming to Georgia Tech, he served on the technical staff of the NASA Langley Research Center for 16 years where he contributed to the design, development, test, and operation of several robotic space flight systems. He has worked extensively in the areas of entry system design, planetary atmospheric flight, and mission architecture development. Dr. Braun is an AIAA Associate Fellow and the principal author or co-author of over 100 technical publications in the fields of planetary exploration, atmospheric entry, multidisciplinary design optimization, and systems engineering. He has a B.S. in aerospace engineering from Penn State University, a M.S. in astronautics from George Washington University, and a Ph.D. in aeronautics and astronautics from Stanford University.

Received 1 August 2005; revision received 7 December 2005; accepted for publication 13 December 2005.

*Graduate Research Assistant, Guggenheim School of Aerospace Engineering, 270 Ferst Drive. Student Member AIAA.
†David and Andrew Lewis Associate Professor of Space Technology, Guggenheim School of Aerospace Engineering, 270 Ferst Drive. Associate Fellow AIAA.

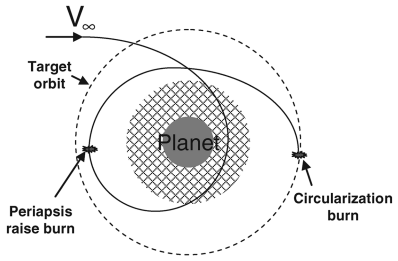

Fig. 1 Aerocapture mission profile.

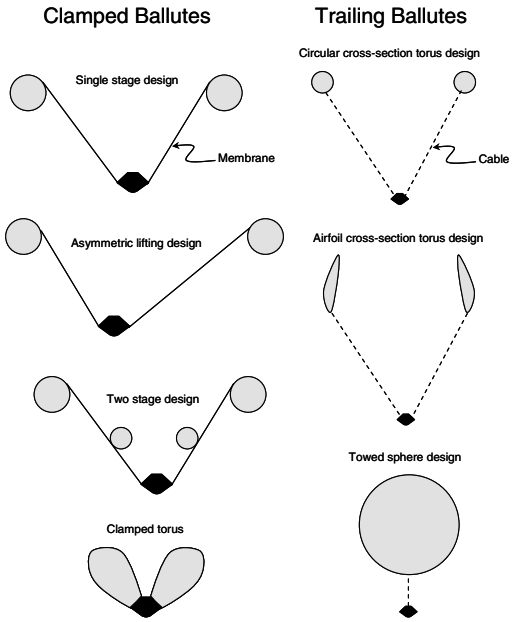

Fig. 2 Examples of clamped and trailing ballutes.

deceleration and heating (both heat rate and heat load) than aerobraking due to the large velocity reduction achieved in a single pass.

The Goodyear Aerospace Corporation coined the term "ballute" (a contraction of "balloon" and "parachute," which the original ballute closely resembles) for their cone balloon decelerator in 1962 [3]. The term has become popular in the literature and now typically refers to any inflatable drag device for high speed deceleration. In the present literature ballutes are divided into clamped and trailing types, as illustrated in Fig. 2.

In 1982, Walberg reviewed the aeroassist state of the art, including aerocapture for planetary entry and orbit insertion [4]. Missions to Mars, Saturn (via Titan aerocapture), Uranus, and Venus were reviewed, and all showed significantly reduced launch mass compared with an all propulsive mission (often by a factor of 2).

In [5] several missions are identified from the NASA Space Science Strategic Plan[‡] that require orbital insertion or entry at planets with atmospheres, and that could benefit from the mass savings of aerocapture. Mass savings of more than a factor of 2 for the orbit insertion system are realized for these missions with incorporation of thin-film ballute technology. Hall and Le [5] also demonstrate that a significant entry corridor exists for each mission where the steep entry limit is the material temperature limit and the shallow entry achieves the required velocity decrement without releasing the ballute. Three common materials for ballutes are carbon fiber, fiberglass, and Kapton, which maintain sufficient strength up to temperatures of about 3500, 850 and 500°C, respectively. In [6], Hall et al. compare the mass and cost of aerocapture to chemical propulsion, chemical propulsion with aerobraking, and solar electric

[‡]Data available on-line at http://www.hq.nasa.gov/office/codez/plans/SSE00plan.pdf [cited 17 June 2005].

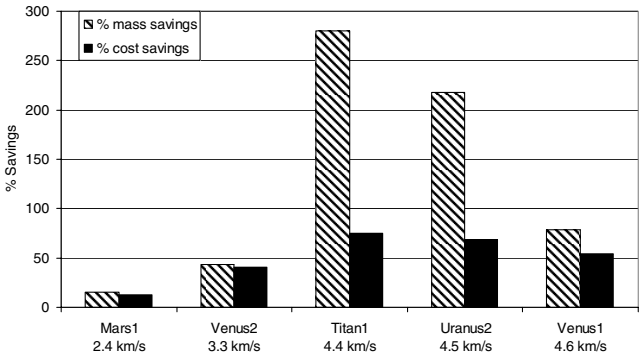

Fig. 3 Mass and cost savings using rigid aeroshell aerocapture [6].

propulsion options. Ten planetary missions are studied and include insertion into circular and highly elliptic orbits at each feasible body. The study concludes that aerocapture is enabling for three missions ($\Delta V = 6$–17 km/s), enhancing for five missions ($\Delta V =$ 2.4–4.6 km/s), and not helped by two of the missions ($\Delta V \leq$ 1.4 km/s). Figure 3 shows the mass and cost savings afforded by aerocapture over the best nonaerocapture option for missions enhanced by aerocapture. Rigid aeroshells are used for aerocapture at all planets.

A. Early Ballute Development

The instability and low drag of supersonic parachutes [7] and the desire to recover high-speed, high-altitude payloads led to the testing of towed spherical balloons as high-speed drag devices by McShera and Keyes [8] in 1961. Many other early tests and studies demonstrated the good supersonic stability characteristics of the ballute [9–14].

The advantages of the low ballistic coefficient were used in [15] as a supersonic decelerator for Mars entry. Both trailing and attached ram-air inflated configurations constructed of Nomex or Dacron cloth coated with Viton or Neoprene were considered. A range of entry conditions were considered with a target of reaching Mach 1 at 20,000 ft altitude. All configurations were able to meet the target altitude for material temperatures less than 230°C encountered when deployed at speeds up to Mach 5. In 1968, Alexander reviewed the test envelope of clamped fabric ballutes [12]. Tests were conducted with metal ballutes up to Mach 10, but fabric ballutes were not tested at conditions exceeding Mach 3 flight conditions. In [16] the drag characteristics of the ballute and parachute are summarized as a function of Mach number, and ballutes are shown to be more effective decelerators than parachutes at speeds above Mach 1.5. The mass delivery advantage of using a supersonic clamped ballute is shown in [16,17] for Mars entry. Mass advantages in excess of 15% are discovered when deploying a clamped fabric ballute at Mach 5 in place of a parachute at Mach 2.

Recognizing the potential mass and operational advantages of a ballute system, Andrews and Bloetcher [18] and Grenich and Woods [19] proposed ballute concepts for aerocapture. Heitchue [20] first proposed the use of a clamped ballute for entry from orbit in 1963 as a single-use personal space rescue vehicle. The concept consisted of a flight seat for a space-suited astronaut around which a clamped ballute inflated. The system was designed to land without a parachute and used an inflatable pad to limit impact acceleration. The concept was later expanded and refined for recovery of both men and payload in [21–23].

B. Ballute Aerocapture

Traditionally, aerocapture has been analyzed using a rigid aeroshell similar to those used for entry applications [24,25]. Lift is necessary to control the energy dissipated in the atmosphere in the presence of uncertainties, and so axisymmetric shapes are flown at an angle of attack. French and Cruz [26] showed that an L/D of about 1.5 maximizes the accuracy of the atmospheric exit conditions. References [27–32] show that sufficient accuracy can be achieved with low L/D vehicles ($L/D = 0.3$) for Earth and Mars applications.

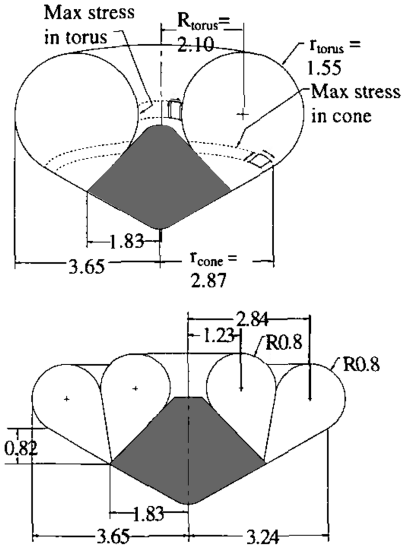

Fig. 4 Clamped ballute configurations for Mars entry with dimensions in meters [33].

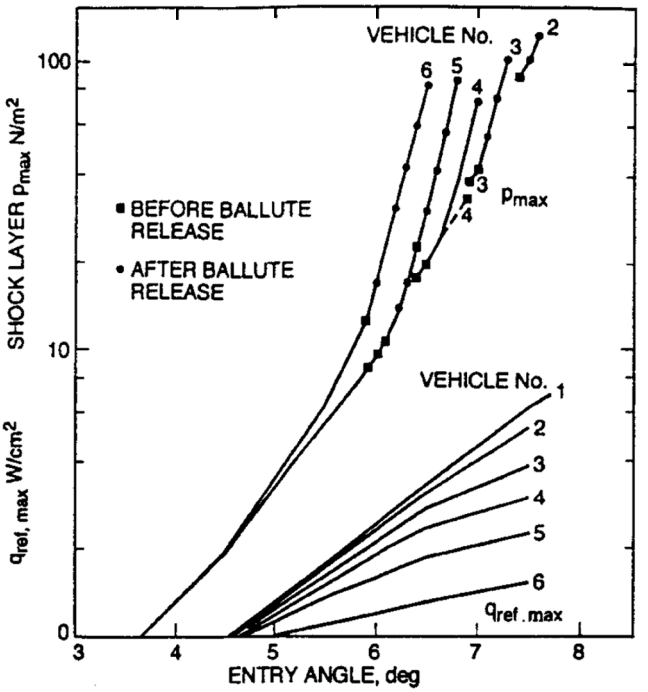

Fig. 5 Peak heat rate and pressure for spherical ballute aerocapture at Mars [35].

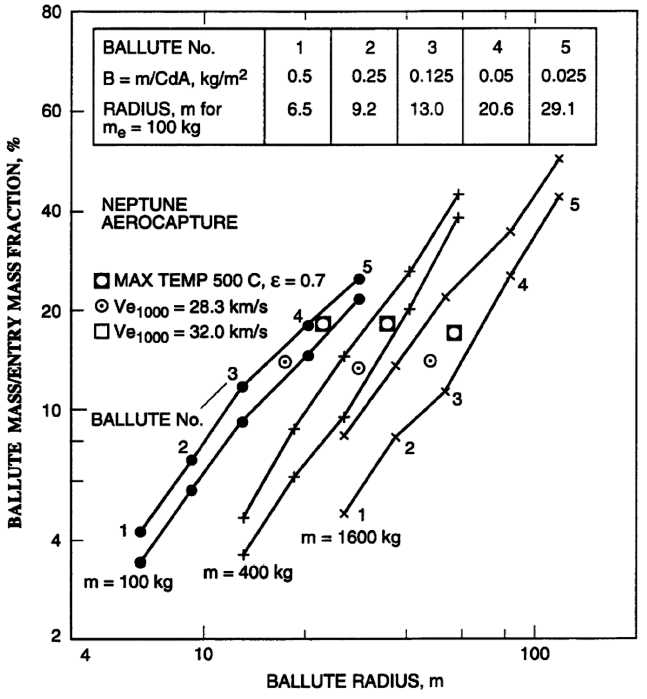

Fig. 6 Ballute mass fraction (ballute mass/entry mass) for Neptune aerocapture [40].

In [4], Walberg points out that one of the most difficult implementation aspects of aerocapture mission design is packaging an orbiter's deployable components inside a rigid aeroshell. To mitigate the packaging concerns of a rigid aeroshell, early ballute aeroassist studies used a clamped, coated Kevlar fabric ballute with a forward facing rocket engine to produce a low enthalpy boundary layer over the vehicle. The center of pressure of this configuration allowed a more aft center of gravity (CG), and the less restrictive geometry made packaging easier. These early studies focused on reducing the orbital energy from geosynchronous Earth orbit to low Earth orbit. Andrews and Bloetscher [18] showed that drag could be varied using engine throttling. Because this would impose a mass penalty, variable inflation pressure was specified instead. Even with the low enthalpy boundary layer produced by the engine, the Kevlar fabric required a quartz outer layer and insulation to maintain its structural integrity.

Kustas et al. [33,34] have explored the clamped ballute configuration for Mars entry. The configurations considered consist of single and double attached toroids as shown in Fig. 4. Trajectory analysis indicates a peak heat rate of 35 W/cm^2 and a multilayer insulation strategy is specified to protect the spacecraft and ballute. Kustas et al. show a mass savings of 43% over a traditionally designed SLA-561V heatshield of the same size.

The low β of ballute aerocapture results in deceleration higher in the atmosphere and with significantly reduced heating rate on the spacecraft. In [35], McRonald used this principle to design ballutes for entry and aerocapture at Mars and Pluto, and discovered that a ballute with a diameter 10 times that of the spacecraft (resulting in a β 100 times lower than that of a rigid aeroshell) could realize a heat rate 100–10,000 times less than with a rigid aeroshell.

Figure 5 shows the heat rate for a Mars mission using a ballute for aerocapture. The lower curves are for heat rate and the upper curves are stagnation pressure. The vehicle numbers represent spherical towed ballute/spacecraft combinations with β decreasing from 5 to 0.05 kg/m^2 for vehicles 1–6, respectively. As noted previously, lower β leads to lower heat rate. Heating rates below 4.0 W/cm^2 are readily obtained for a ballute whereas heating rates of near 40.0 W/cm^2 are obtained for rigid aeroshell aerocapture [36]. The reduced heat rate eliminates the need for an ablative thermal protection system (TPS) encompassing the spacecraft and relaxes packaging requirements. Furthermore, this low heat rate allows materials to be radiatively cooled to around 500°C.

Yavrouian et al. [37,38] present properties of polybenzoxazole (PBO), polyimidobenzoxazole, Mylar, and Kapton thin-film polymers at temperatures up to 500°C for balloon applications on Venus. These materials are also well suited for ballute construction. Entry and aerocapture at Venus and Neptune are examined in [39,40] with ballute systems constructed of PBO and Kapton. Analysis at all four planets shows that ballute mass to entry mass fractions can be in the 10–20% range. Figure 6 demonstrates the ballute to entry system mass fractions possible for aerocapture at Neptune. Two other ballute configurations were examined by McRonald, the lenticular and toroidal ballute, which are depicted in Fig. 7 and have the goal of reducing the inflation gas mass compared with the spherical ballute.

C. Ballute Aerocapture Technical Challenges

Despite the promising outlook portrayed in papers by McRonald [35,39,40], Hall and Le [5], and Kustas et al. [33,34], much of the

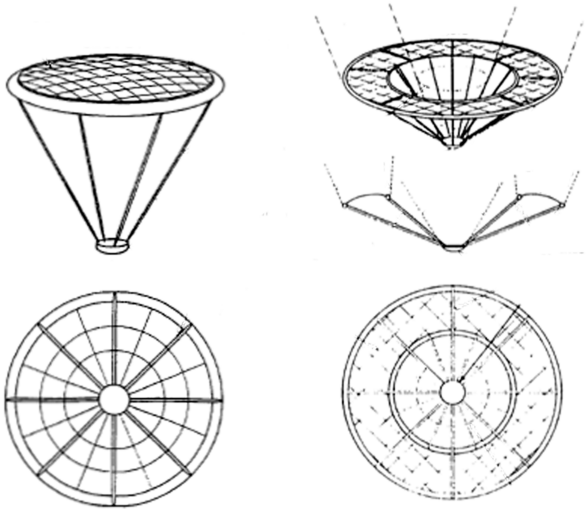

Fig. 7 Lenticular (left) and toroidal (right) ballutes designed to reduce inflation gas mass [35,40].

ballute analysis has been at the conceptual design level with little subsystem work to better define system mass and implementation options. Recognizing that more detailed work was needed, Hall [41] reviewed the state of ballute technology for planetary aerocapture in 2000 and summarized the current state of ballutes for planetary aerocapture with 10 key technical issues. A summary follows.

Determination of optimal ballute shape was identified as the number one issue surrounding ballute aerocapture. Several ballute shapes have been proposed in the literature, including trailing spheres, trailing toroids, clamped spheres, and clamped toroids. Issues include tether heating for trailing ballutes, system mass, flow stability, and drag characteristics. Flow stability is closely tied to ballute shape, with instabilities being observed in early tests of trailing and clamped ballutes. Large scale flow instability, such as vortex shedding, can cause motion and orientation changes of the ballute/spacecraft system. Smaller scale instability has also been discovered due to shock-shock interaction. Preliminary results suggest that this can be avoided by using a toroid of proper geometry, but further studies are needed. So far studies have assumed ballutes are rigid, but aeroelastic phenomena need to be explored.

Survivability of the ballute system needs to be addressed in more detail. Material strength at temperature needs to be addressed in a trade including inflation pressure, size, and heat rate. It is unknown if thin-film materials will be strong enough in the applicable flight regime. Expanded material testing is needed, and more accurate heat rates are needed to determine actual material temperature, including the impact of radiative heating on these large configurations. Trailing ballutes have the further complication of tethers between the spacecraft and ballute. Tether materials must handle higher heat rates than the ballute itself (due to a smaller effective nose radius) and shock impingement from the tethers must not cause localized heating above the material temperature limits on the ballute. Even though dynamic pressure and heating is low compared with rigid aeroshells, ballute materials are more fragile to achieve mass benefits. Given the high temperature and lightweight materials, can a ballute be designed that can handle the large drag forces?

Preliminary results indicate significant mass savings over both propulsive orbit insertion and rigid aeroshell aerocapture, but more detailed analysis is necessary. Changes in ballute shape, size, or inflation pressure could have a significant impact on the system mass.

Parent spacecraft protection is of paramount importance, and because the spacecraft is small relative to the ballute, the heat rates are higher. If the heat rate on the spacecraft is too high, TPS will be necessary, cutting into the packaging and mass benefits provided by the ballute. Furthermore, if the heat rate becomes too high on the ballute, how do you protect a flexible, deployable structure?

Trajectory robustness is needed to demonstrate a high probability of success. Control algorithms need to be developed and tested to demonstrate their accuracy and robustness. Because the atmosphere is the primary source of uncertainty, better models are needed, which will likely require more atmospheric measurements. Large uncertainties will still exist, and control algorithms will need to be able to handle large atmospheric variation to maintain adequate margins.

Deployment and inflation of a large structure has been attempted only once (on the Inflatable Antenna Experiment), and that was a mixed success. Deployment and inflation was achieved, but not through the expected means because residual gas caused premature deployment of the structure. Lessons can be learned from the Inflatable Antenna Experiment [42], but additional work needs to be done to avoid tether tangling and to explore the effects of long storage times. The inflation system also needs a mechanism to avoid overpressure as the gas expands during the atmospheric pass.

Experimental verification of ballutes is difficult, particularly for deployment and aerothermodynamics. Gravity and aerodynamic drag alter the results of laboratory deployment testing, and for planetary missions the complete aerothermodynamic environment cannot be reproduced on Earth. Computational tools exist for analysis of ballutes, but verification and validation in a relevant flight environment is often cost-prohibitive or impossible at Earth. This leaves two questions: What combination of testing and analysis is sufficient to prove the concept, and can the appropriate scaling parameters be matched in any existing facility?

The remainder of this paper will survey the technology applicable to the ballute aerocapture problem. The majority of studies reviewed have been published since 2000, but some that seem particularly relevant are from earlier dates. The work has been separated into sections on trajectory analysis, structural analysis, hypersonic aerothermodynamics, coupled analysis, and flight tests.

II. TRAJECTORY ANALYSIS

During 2003 and 2004 a significant amount of work was performed to determine the aerocapture capability of ballutes at Titan. Miller et al. performed a systems study based on the toroidal trailing ballute. In [43] they detail the analysis, including configuration and spacecraft packaging, aeroheating in the continuum, transitional and free-molecular flight regimes, and thermal and trajectory analyses. An aerodynamic database was developed for a 5:1 (R/r) torus and was used for trajectory analysis. Titan atmospheric entry was initiated at 1000 km altitude, at 6.5 km/s velocity, values typical of a low-thrust trajectory to the Saturnian system. For comparison, Mars aerocapture trajectories were also investigated, with a nominal entry velocity of 5.5 km/s at 200 km altitude. For Titan and Mars, β was 0.4 and 0.8 kg/m^2, respectively. Table 1 lists the critical points in the trajectory for both Mars and Titan aerocapture. Titan trajectory work was extended to include an algorithm for ballute release. The algorithm uses orbital energy as the release criteria and propagates the trajectory onboard using accelerometer data and an updated density model. A Monte Carlo analysis was performed with perturbations to the atmosphere, accelerometer data, entry velocity, entry flight path angle, and β. The resulting circularization velocity increment and heating values are presented in Table 2. Two other sources [44,45] have implemented algorithms for ballute release at Titan and performed Monte Carlo analysis showing similar performance.

In [46], Lyons and Johnson studied the trailing toroidal ballute for Neptune aerocapture into a highly eccentric orbit with apoapsis at

Table 1 Comparison of Mars and Titan aerocapture trajectories [43]

Characteristic	Mars	Titan
Ballute β, kg/m^2	0.8	0.4
$\beta_{\text{spacecraft}}/\beta_{\text{ballute}}$	140	145
V_{entry}, km/s	5–6	6–8
Pass duration, s	1100	3600
Velocity decrement, km/s	2.0	4.8
Peak deceleration, g	2.8	4.3
Peak heat rate, W/cm^2	2	0.9
Peak heat rate, Pa	28	46

Table 2 Results of Monte Carlo simulation of Titan aerocapture trajectory [43]

Characteristic	Value
Number of failed[a] cases	0
Min. circularization ΔV	125 m/s
Max circularization ΔV	376 m/s
Mean circularization ΔV	186 m/s
Mean + 3σ circularization ΔV	285 m/s
Mean heat rate	1.9 W/cm^2
Mean + 3σ heat rate	2.1 W/cm^2

[a]Failure is entering, or not capturing.

430,000 km. This study assumed a 500 kg spacecraft and explored three ballute sizes (750, 1477, and 3000 m^2) and seven entry velocities (22.4, 22.8, 23.4, 24.1, 25.0, 26.1, and 27.2 km/s). Figure 8 shows the maximum heat rate on the ballute for the range of entry velocities. Peak heat rate varies between different ballute areas by roughly a factor of 2 for low entry velocities, and by more than a factor of 5 for high entry velocities. Larger ballutes at lower entry speeds are advantageous from a heating perspective. Trajectories in this study were targeted independently such that the exit conditions were met without releasing the ballute. Because this method did not account for uncertainties, the heat rates shown would increase once a lower periapsis is targeted to account for uncertainties. Peak deceleration is shown to be 3.5 g, but again will increase slightly once uncertainties are accounted for. Even if the deceleration increased by 40%, the deceleration would still be less than 5 g, a tolerable level for instruments and even humans. The study concludes that heat rate is the driving factor in ballute design for Neptune entry given the high entry velocities. An effort should be made to design a mission which reduces the arrival velocity so that heat rate can be maintained within the limits of thin-film materials for reasonable size ballutes.

Ballute aerocapture trajectories have been explored thoroughly for a 500 kg spacecraft at Titan. A robust algorithm has been developed that successfully inserts the spacecraft into orbit using drag modulation while accounting for uncertainties. Preliminary analysis at Neptune and Mars is also presented and shows that a sufficient entry corridor exists to account for uncertainties. The algorithm presented in [43] needs to be adapted to other atmospheres, or new ones developed, to verify the ability to perform ballute drag-modulated aerocapture at other planets.

III. STRUCTURAL ANALYSIS

Structural analysis of early inflatables was largely based on empirical results and application of simple membrane equations. In 1964, the membrane equations were manipulated by Houtz to show that a uniform stress fabric reinforced with meridian cords could be designed for a given axially symmetric pressure load. In [47], he shows the technique by which the meridian profile, number of meridian cords, and fabric gore shape could be designed using algebra and integration. For a sphere, a meridian cord would follow a line of longitude, and a gore would be the surface pattern between two lines of longitude as shown in Fig. 9 for a clamped ballute.

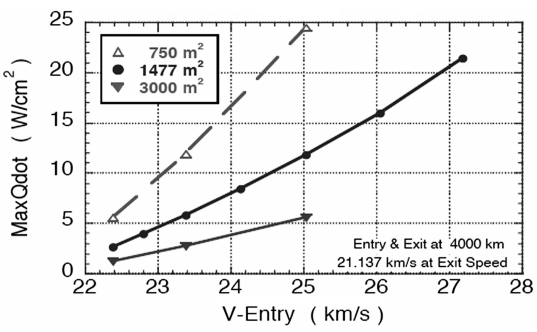

Fig. 8 Peak heat rate on a trailing toroidal ballute at Neptune [46].

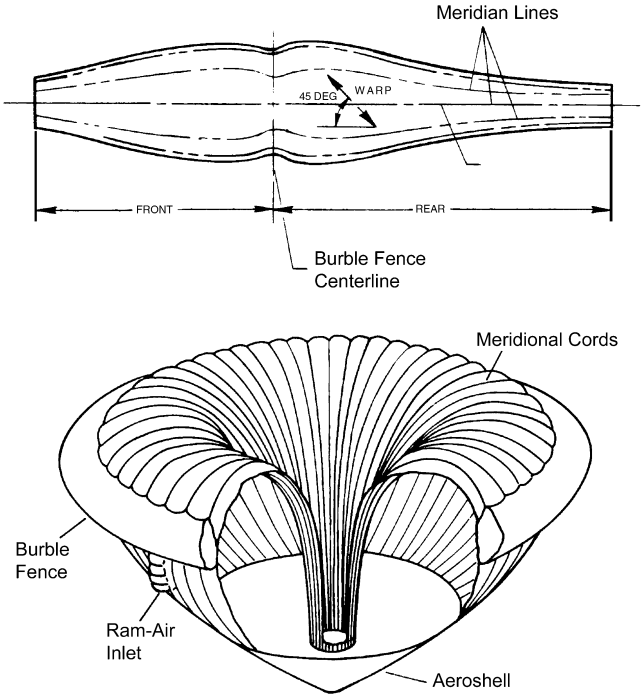

Fig. 9 Clamped ballute showing the meridian cords and a gore pattern used in its construction [84].

Solutions to the differential equations are families of curves dependent on the axial load factor and meridian cord factor. When σ is zero the solution has zero slope at the axis, and when k is zero too, the surface becomes a sphere with uniform stress in all directions. When σ is zero and k is one the stress is carried completely in the meridians. These two cases are the bounding curves in Fig. 10 for a constant pressure load which is typically used for aft surfaces. Here the y-axis is the axis of symmetry and dimensions have been normalized by the base radius of the vehicle. For forward surfaces, the pressure distribution is fixed and the surface shape must be solved. Though not stated in the paper, it would clearly be necessary to iterate between the actual shape obtained and the pressure distribution to achieve a consistent solution. Isotensoid design became the de facto method for ballute design in the latter half of the 1960s.

Also in 1964, Anderson [48] identified that aeroshell design is limited by the buckling load case, so the full strength of materials is not used. This led to the concept of the tension shell entry vehicle where the compressive load is isolated in a single ring structure at the base of the vehicle. Anderson also demonstrates that the tension shell

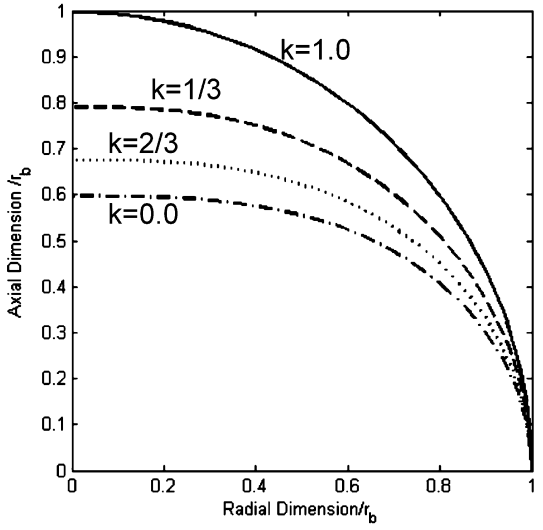

Fig. 10 Surface curves for $\sigma = 0$ and constant pressure load [47].

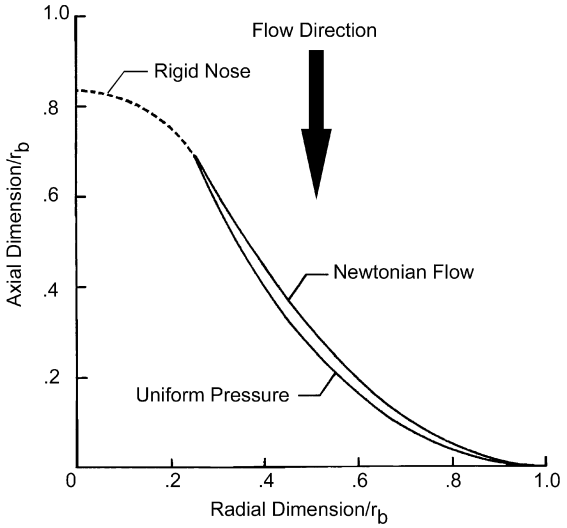

Fig. 11 Tension shell surface shapes for Newtonian and constant pressure distributions [49].

shape can achieve a lower ballistic coefficient than a rigid aeroshell. In [49] the shape is mathematically defined using membrane theory and both a constant and Newtonian pressure loading. The surface contours for each pressure loading are shown in Fig. 11 for solutions with the same end points. The vertical-axis is the axis of symmetry with dimensions normalized by the base radius. The flow direction is from top to bottom. The small difference in the contours indicates that the shape is not sensitive to the pressure distribution because the Newtonian and constant pressure distributions are quite different. From the pressure distribution it was found that for relatively blunt versions of the tension cone the drag coefficient is between 1.4 and 1.7.

Because the tension shell required no compressive strength, a thin fabric or membrane could be used as the aerodynamic surface. To achieve very low ballistic coefficients the surface could be deployed using an inflatable torus to support the compression load. In 1967, the equations for buckling of a radially loaded pressurized toroidal shell were developed [50]. These equations were then verified and used in [51] to analyze the deployment and flight of a tension cone. For verification purposes two fixtures were used to apply a distributed radial load to the torus: a toggle harness and a vacuum bag apparatus. Both a slender ($R/r = 7.25$) and a stout torus ($R/r = 4.71$) were tested in each fixture, and three compressive failure modes were identified. The first failure mode is when the circumferential load in the torus due to the radial load P exceeds the circumferential force in the torus due to pressure:

$$P > p\pi r^2 \tag{1}$$

This failure mode was termed the crippling mode and was characterized by a wrinkling of the torus surface followed by the torus folding, out-of-plane, about a single hinge line. The remaining two failure modes are in-plane and out-of-plane buckling modes. The out-of-plane buckling mode appeared as a curling deformation and was able to support an increasing load until the crippling load was reached. The in-plane buckling mode appeared as four hinges and four arcs as shown in Fig. 12. The buckling load as a function of internal pressure for the slender torus, shown in Fig. 13, is in good agreement with theory. For the stout torus the results are similar, except that the wall has a larger contribution to the compressive strength, hence collapse is observed consistently at loads greater than the crippling load.

Kyser [51] also developed a model for deployment of an inflated torus based on a hinge moment when the torus is folded, out-of-plane, in half. The model was applied to a tension shell decelerator and tested in a water tow tank. Results indicated that the theory is conservative as complete deployment was observed at lower fill pressures and higher dynamic pressures than predicted. It should also be noted that the surface shape was designed using a Newtonian

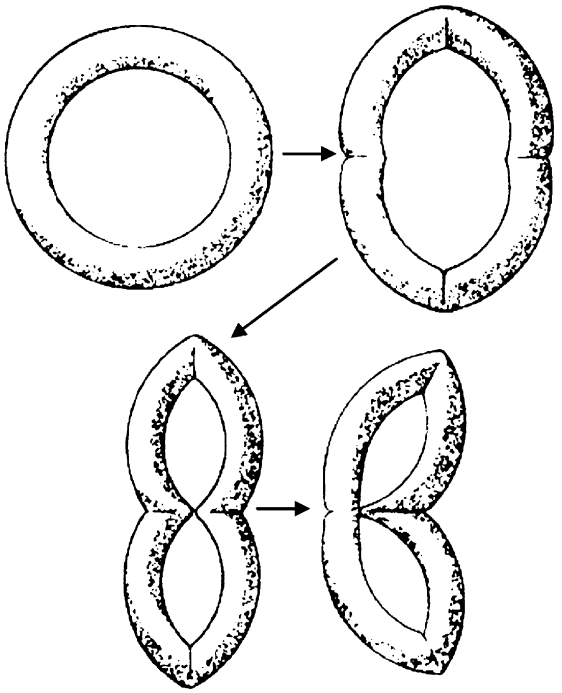

Fig. 12 Planar buckling mode of a pressurized toroidal shell under uniform radial load [51].

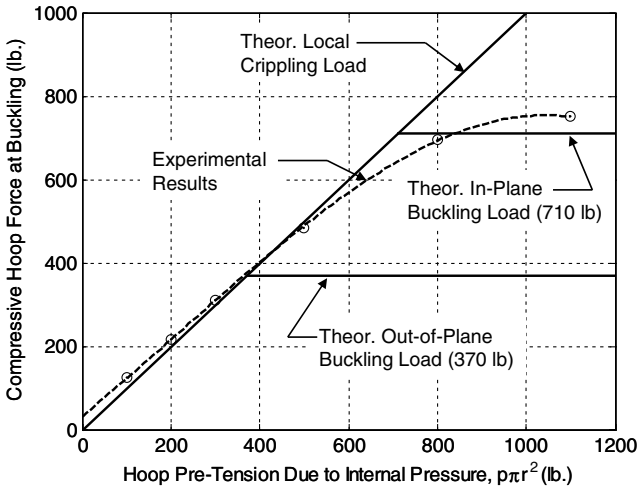

Fig. 13 Experimental buckling load of a slender torus showing good agreement with theory [51].

pressure distribution and produced wrinkles during tow tests, indicating that the actual pressure distribution was far from Newtonian.

In recent years finite element analysis (FEA) has been used to analyze ballutes. Prada y Nogueira et al. [52] detail the analysis of a coated fabric clamped ballute with TPS using FEA. The LS-DYNA structural dynamics code is used to study the deformation due to aerodynamic pressure and the effect of air chamber deflation on two different configurations. The analysis used the fabric material and inflation models developed for automotive airbag analysis.

The NASTRAN and ABAQUS codes were also used to model an inflated cylindrical membrane strut. Modal analysis was performed using each analysis package and the results compared favorably to experiment for the first mode. For higher modes results were not as good, with errors as high as 24%. Within the results for the first mode, better accuracy was achieved for stiffer configurations (thicker membrane and higher inflation pressure). In general the NASTRAN and ABAQUS codes were found to have similar accuracy.

Numerical modeling of thin polymer membranes has presented several difficulties, including numerical instability and accurate

capture of surface wrinkles and deformation. Many of the membrane modeling advances have been made by the solar sail community and are only just starting to be applied to ballutes. In [53], Wang et al. use the ABAQUS code to explore the effects of element formulation and analysis type (implicit vs explicit) on the deformation of a membrane strip under gravity loading. The seemingly simple problem of numerically solving the membrane equations using FEA proves difficult. The implicit solution technique only produced correct results for the membrane element formulation with either stabilization or pre-tension added. Only reduced integration shell elements were able to produce converged solutions, though the results underpredicted the deformation. The explicit solution technique used a reduced integration shell element and produced the correct result with artificial damping added to eliminate oscillations due to the load application method.

The numerical prediction of surface wrinkle amplitudes in a true membrane is not possible due to the influence of bending and compressive stiffness on the shape of the wrinkles. Furthermore, initially flat membranes under shear or compression will not buckle because there is no means to produce a bending moment. This problem was resolved by initially perturbing the nodes by a fraction of the membrane thickness to couple the bending moment to the shear and compressive loads [54]. The method was used to predict wrinkles in a flat membrane subject to a pure shear load and a flat membrane subject to corner tension. The wrinkle patterns in the computational results compare well with experiments, but the amplitudes vary by nearly a factor of 2. Su et al. [55] apply the tension field theory to predict the wrinkle patterns, and nonlinear post-buckling analysis to predict the wrinkle amplitudes in a square membrane with corner loads. Amplitude prediction is quite good for wrinkles away from the edges, but wrinkle amplitudes near the edges are much smaller than those found in testing.

Theories have been developed and validated through tests for pressure stabilized structures in the presence of variable external loads. The analytical methods presented provide the tools for preliminary sizing of both clamped and trailing ballutes. The finite element method has been successfully applied to analysis of coated fabric ballutes and modeling of thin polymer membranes should be possible due to advances made by the solar sail community.

IV. HYPERSONIC AEROTHERMODYNAMICS

Unsteady flow effects have long been observed in parachutes and so it was not surprising to see them in early supersonic ballute tests. McShera and Keyes observed time varying flow separation from the tow cable in [8], and McShera observed failure due to unsteady flow in [10].

Early tests were at supersonic Mach numbers with relatively high dynamic pressures (at low altitude on Earth). In contrast, aerocapture applications encounter only hypersonic flow and low dynamic pressures [56] ($q < 100$ Pa compared to $q > 12$ kPa), but may still suffer failure due to a fluctuating thermal environment or fluid-structure interaction. Computational and experimental studies of ballute aerodynamics have been performed as a series of related studies, with overlapping cases for validation purposes.

A. Experimental Results

Rasheed et al. [57] performed a set of experimental studies using a toroidal ballute. It was thought that the hole in the torus would swallow the spacecraft wake and reduce aerodynamic interaction between the bodies. Because of the resulting small minor radius of the torus, heating was a concern and testing was performed to determine the heating rate on the torus. Heating tests were performed in the Graduate Aeronautical Laboratories, California Institute of Technology (GALCIT) T5 Hypervelocity Shock Tunnel. Test conditions were set to match the reference Reynolds number and stagnation enthalpy similarity criteria for aerocapture of the Mars Microsatellite and the Titan Organics Explorer, two possible applications of a toroidal ballute. The experimentally determined heat rates will be higher than flight conditions due to the high enthalpy flow and small test article dimensions. High enthalpy flow is necessary to capture the effects of flow chemistry and the ensuing change in shock wave geometry. Because of the small geometry, heating due to radiation cannot be captured in shock tube experiments, necessitating a flight experiment to fully simulate the environment. Table 3 shows the design parameters for these two missions. Test results show good agreement with theory for the Stanton number as a function of the Reynolds number, which can be extrapolated to provide heat rates for these missions. Additional tests were performed with the hole of the torus blocked to verify the unsteadiness observed in the computational results [58]. The complex shock shape shown in the experiment indicates the flow was unsteady.

Table 3 Ballute mission design parameters [57]

Design parameter	Mars Microsatellite value	Titan Organics Explorer value
D_{major}, m	15	52
D_{minor}, m	3	13
V_∞, m/s	5490	8550
ρ_∞, kg/m^3	7.1×10^{-7}	1.9×10^{-7}
Gas	95% CO_2	98% N_2

McIntyre et al. [59] extended the work of Rasheed et al. [57] to flows of higher freestream enthalpy to better capture the effects of dissociation and ionization. A moderate enthalpy case ($\sim$18 MJ/kg) in CO_2 and N_2 was studied for comparison to the previous study, and a high enthalpy case ($\sim$50 MJ/kg) was studied to see the effects of dissociation and ionization. Additional testing was performed at high enthalpy ($\sim$80 MJ/kg) in a hydrogen-neon gas to simulate entry into a gas giant. The toroidal ballute model used in [57] was scaled to fit in the University of Queensland superorbital expansion tube, X2. Both a standard torus and a blocked torus model were used to explore the effects of choked flow. In general, it was found that shock interaction occurs further downstream for higher enthalpy and higher Mach number flows. Good agreement between calculated and experimental heat rate was observed for the moderate and high enthalpy N_2 conditions and the high enthalpy CO_2 condition. The flow around the blocked torus was unsteady in all conditions. Table 4 shows a sample of the experimental data obtained and the calculated heat rate and Stanton number for the moderate enthalpy N_2 case. When higher freestream enthalpies were included it was found that the Stanton number still followed the $Re^{-1/2}$ relation found in [57].

B. Computational Studies

In 2001, Hornung [58] performed a series of time-accurate inviscid computational fluid dynamics (CFD) solutions for vehicles with an elliptical and a toroidal towed ballute. The study examined the effect of towing distance and a sting support. The elliptical trailing body was found to have violently unsteady flow for medium towing distances, but steady flow for very short or very long towing distances. Figure 14 shows a pseudoschlieren image at Mach 10 for an elliptical towed ballute at medium distance with unsteady shock structure. Because the unsteadiness in the flow originated from

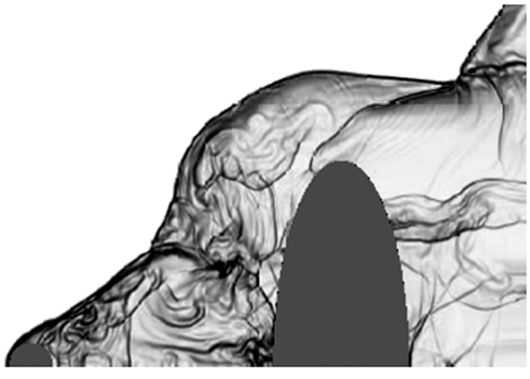

Fig. 14 Unsteady flow over elliptical towed ballute at Mach 10 [58].

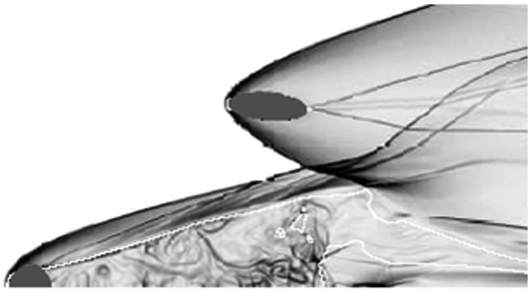

Fig. 15 Steady flow over a sphere towing a toroidal ballute [58].

interaction of the towing spacecraft wake with the shock structure of the towed ballute, it was thought that moving the shock interaction further downstream from the spacecraft would improve the situation. By using a toroidal ballute the towing distance could still be reasonable, and the shock interaction would be moved downstream because it would pass through the hole in the torus. Further computations showed that the spacecraft wake was swallowed, but the shock reflections on the axis of symmetry produced such high pressure that the shock moved upstream to the base of the towing spacecraft, producing unsteady flow in its wake. The addition of a sting supporting the spacecraft significantly reduces unsteadiness and leads to a much more benign environment for the spacecraft.

Because the torus must be connected to the spacecraft with a tension device, it would be convenient to counter the radial force of the tethers with outward lift from the torus. An outward radial force can be provided by giving the torus an elliptical cross section with an angle of attack. Analysis of this configuration yielded the steady shock structure shown in Fig. 15. The effectiveness of a ballute can be based on the mass required to achieve equivalent drag. Analysis of the elliptical and toroidal ballutes shows that the primary difference is in the inflation gas, with the toroidal ballute requiring about one quarter the volume of the elliptical ballute.

Computational studies using the LAURA [60] algorithm were performed in [61] for one of the toroidal ballute cases (torus only) at Mars used in [57] (case T2018-toroid) to validate the computed heating rate. The computational models include viscous and real-gas effects [62]. To capture the real-gas effects, the validation experiment used a high enthalpy flow with a scale model, resulting in heat rates significantly higher than expected in flight. Three different boundary conditions were analyzed with the experimental data being bounded by the fully catalytic wall and the fully catalyzed atomic oxygen only cases, except near $\theta = 90$ deg. Figure 16 shows the experimental data along with the three computed heating rates. Drag coefficients for toroidal and spherical ballutes are also calculated in the Venus, Saturn, Titan, and Neptune atmospheres.

Additional computational studies of toroidal and spherical trailing ballutes were performed by Gnoffo and Anderson using the LAURA algorithm in the Titan atmosphere [63]. Studies of a trailing toroidal ballute found that a steady solution exists with no flow impingement on the aft of the spacecraft. The same model run with an increased Reynolds number produced a much stronger interaction which enveloped the base of the spacecraft as in [58], but the solution had only small oscillations present near the base of the spacecraft. Even with flow impinging on the aft end of the spacecraft there was no unsteady flow interaction with the ballute. The increased heat rate on the spacecraft could easily be countered by addition of TPS to the spacecraft backshell.

For the trailing spherical ballute studies, the same 6-m-diam spacecraft was used, and a 70-m-diam sphere was towed at distances ranging from zero to 200 m (0, 30, 40, 50, 100, 200 m). For towing distances between 30 and 200 m the peak drag produced by the ballute occurs at a tow line length near 50 m. For the longer towing distances the ballute is almost completely enveloped in the low dynamic pressure of the spacecraft wake, producing significantly less drag. In the 30–200 m towing distance there is a significant increase in heat rate on the ballute where the spacecraft bow shock intersects the inflated sphere. In all computational cases, a steady state flow resulted for the baseline conditions, and a recirculation zone was present in front of the sphere for tow distances between 30 and 100 m. As with the toroidal ballute, a tenfold increase in Reynolds number produced marginally unsteady flow with upstream flow extending to the base of the spacecraft for the 40 m towing distance, similar to that observed for elliptical ballutes in [58]. For the limiting case of zero tow distance the spacecraft is protected within the shock layer of the ballute, resulting in lower heat rates.

Figure 17 compares the convective heating rate on the clamped ballute configuration to the sphere and spacecraft individually. The lack of shock interactions, unsteady flow, and reduced heating rates make this an attractive option. In the analysis of both the toroidal and spherical ballutes the wake flow had a Knudsen number of order 1 or higher, invalidating the continuum solution. Future work needs to include a mixed continuum and transitional regime solution in these areas.

In 2004 Anderson studied the static stability and effects of transitional flow on a spherical, clamped ballute [64]. Static stability was determined from a three-dimensional continuum solution at 5 deg angle of attack. It was found that the clamped ballute was statically stable ($\partial C_m/\partial\alpha < 0$). The effects of transitional flow on the ballute were determined by using a direct simulation Monte Carlo solution. The resulting heat rate falls between the continuum solution for a perfect gas with $\gamma = 1.2$ and a thermal nonequilibrium gas with $\gamma = 1.4$, and is shown in Fig. 18.

The premise of achieving lower system mass through increased size, lower β, and lower heat rate is questioned by Park in [65]. He points out that radiative heating has not been considered, and whereas convective heat rate decreases with increasing size, radiative heat rate is proportional to shock standoff distance, and so

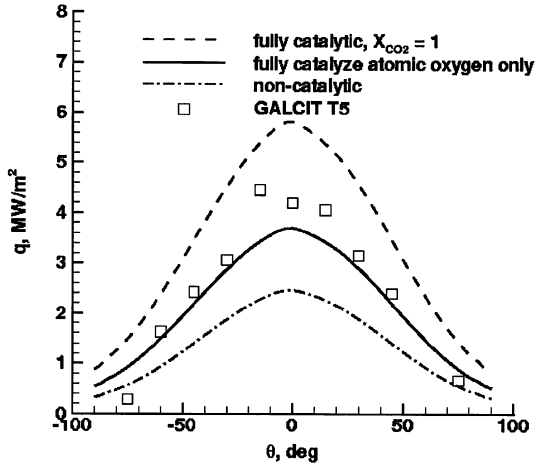

Fig. 16 Heat transfer on the wall of a toroidal ballute in CO_2 computed by LAURA and measured in the GALCIT T5 shock tunnel [61].

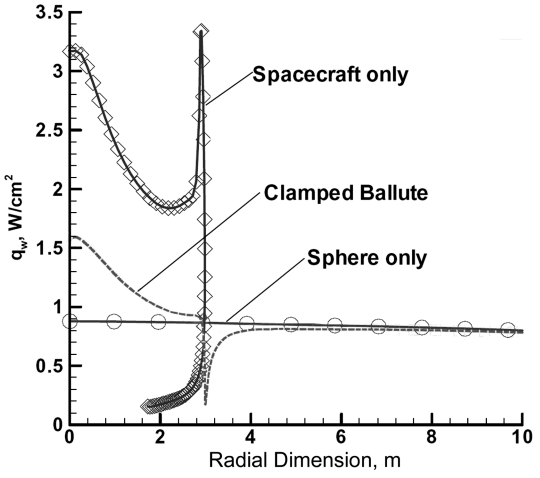

Fig. 17 Heat rate on a clamped ballute and its individual components [63].

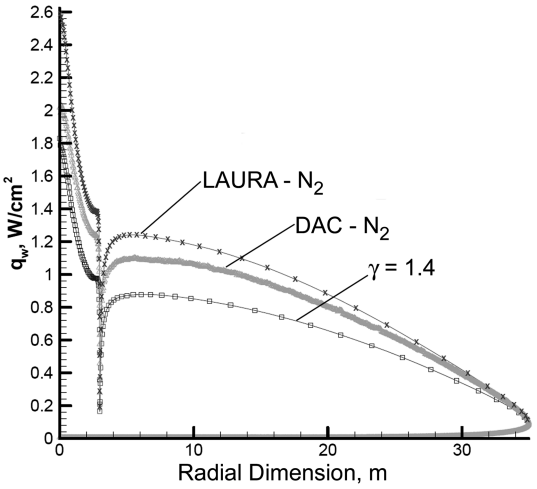

Fig. 18 Effects of transitional flow on the surface heat rate to a clamped ballute [64].

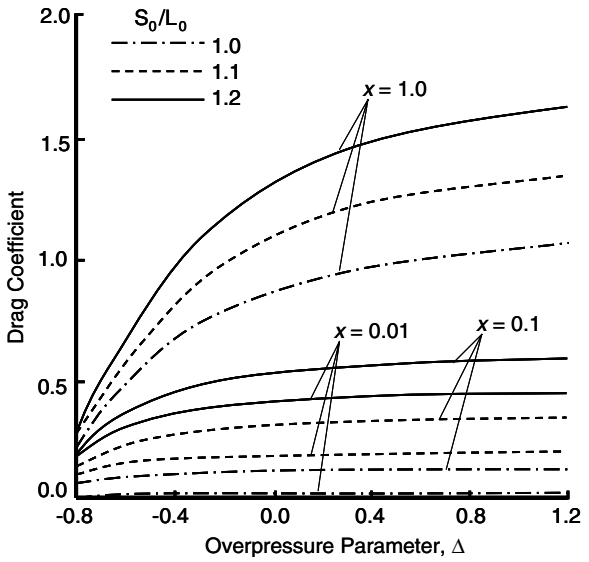

Fig. 19 Variation in C_D as a function of overpressure and elasticity ratio [66].

increases with vehicle size. Park reviews the radiative heat rate observed in ground and flight tests and the theories for predicting radiative heat rate. Using the best theory available (in 1987), the radiative heat rate for Earth return from geosynchronous Earth orbit ranges from 2.5 to 7.0 W/cm^2 for nose radii of 3 and 12 m, respectively, with the rate increasing by a factor of 2.4 for lunar return. This level of heat rate input would be problematic for many candidate ballute materials and would drive the system to larger diameters. Clearly, additional work is needed to determine radiative heating for the Earth and other atmospheres, and these effects must be factored into ballute system design.

The work done in the area of hypersonic aerothermodynamics has shown that unsteady flow exists for simple (spherical and elliptical) trailing ballutes, but can be avoided by using a toroidal trailing ballute at low Reynolds numbers or a clamped ballute. Testing has verified the convective heat rate predictions of the computational methods currently in use. Estimation of radiative heat transfer at high altitudes and for nonterrestrial atmospheres remains a major issue. Further work is necessary to determine the effects of rarefied and transitional flow in the wake of trailing ballutes, and at higher altitudes.

V. COUPLED ANALYSIS

Recognizing that structural shape and aerodynamics are coupled, Park simplified the ballute to a two-dimensional problem and found a set of differential equations subject to constraints that defined its shape [66]. This set of equations was integrated numerically for a given angle of attack, ballute geometry, internal pressure, and material elasticity to find the aerodynamic parameters. Using an analytical approach enabled Park to study the possibility of using internal pressure to control drag. Figure 19 shows the variation in drag coefficient as a function of the overpressure parameter and pressure to elasticity ratio at 0 deg angle of attack.

$$\Delta = \frac{p}{\rho U^2} - 1 \tag{2}$$

$$x = \frac{L_0}{\phi} V^2 (1 + \Delta) \tag{3}$$

For small values of x, the membrane stiffness dominates, and there is little change in the ballute drag, but when x is 1, drag varies by a factor of 5. Therefore x must be of order 1 or greater to use internal pressure to control ballute drag.

An aerocapture trajectory was calculated using planar translational degrees of freedom and one rotational degree of freedom. The trajectory was run with the CG at 0.3000, 0.4375, and 0.4438 times the vehicle length and a small initial angle of attack. The two cases with the CG closest to the nose were stable, but the case with CG $= 0.4438L_0$ became unstable and started to tumble in the low density atmosphere. For stability at all freestream densities the CG must be less than $0.18L_0$. Placing the CG at $0.18L_0$ is very restrictive, but subsequent trajectory work showed that the ballute's dynamic motion was bounded up to CG $= 0.4375L_0$ because the relatively short time spent in the low density region of the atmosphere does not allow the aerodynamic instability to propagate significantly.

With the advent of numerical solutions to the Navier–Stokes equations and the increase in computer speed in the late 1970s and early 1980s, the use of CFD emerged. Abe [67] used CFD to iteratively determine the surface shape of a tension shell vehicle. For this study, an axisymmetric CFD solution was used to determine the pressure distribution. The pressure distributions showed good agreement with experimental results, but poor agreement with Newtonian theory at Mach 7. The discrepancy is due, in part, to separated flow for models with large nose radius relative to base radius, which Newtonian theory cannot capture. The iterative method used to achieve a consistent solution converged in less than four iterations and consistently produced a shorter (more blunt) shape than the initial guess using a uniform pressure distribution. Figure 20 shows a representative example of the surface pressure and shape after each iteration.

The next major advance in modeling of ballutes was the time-accurate coupling of computational structural dynamics (CSD) and CFD. Mosseev [68] presents a coupled solution for the deployment of a trailing ballute at Mach 2 and its final shape using the MONSTR code. The MONSTR code combines a fabric shell structural dynamic solution with three different continuum flow solvers capable of handling moving boundaries. The technology is applicable to any thin, flexible body and Mosseev [69] compares the numerical solution for surface pressure and aerodynamic coefficients to experimental data for several parachutes and a supersonic ballute. The results are quite accurate for the subsonic and low supersonic flight regimes examined. Whereas the code appears capable of transient solutions, the flight condition was fixed for the analysis presented.

Aeroelastic analysis of ballutes poses many challenges, including 1) coupling of a highly flexible structure, 2) nonlinear fluid and structure behavior, 3) FEA of highly nonlinear membranes, and 4) experimental validation of results [70]. Bartels et al. propose wind tunnel tests utilizing the NASA Langley Transonic Dynamics Tunnel to explore the effects of model scale and construction techniques and a computational effort. The computational effort will focus on coupling a nonlinear FEA code to a hypersonic aerothermodynamic code using loose coupling for static solutions and closely coupled modal methods for dynamic solutions. Because of large computational requirements, system identification and order

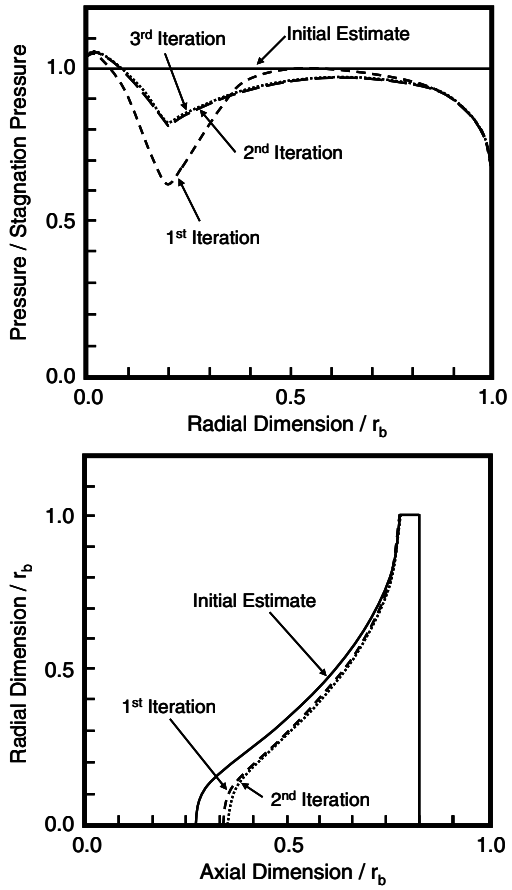

Fig. 20 Iteration history of pressure distribution (top) and vehicle shape (bottom) for a consistent tension shell vehicle [67].

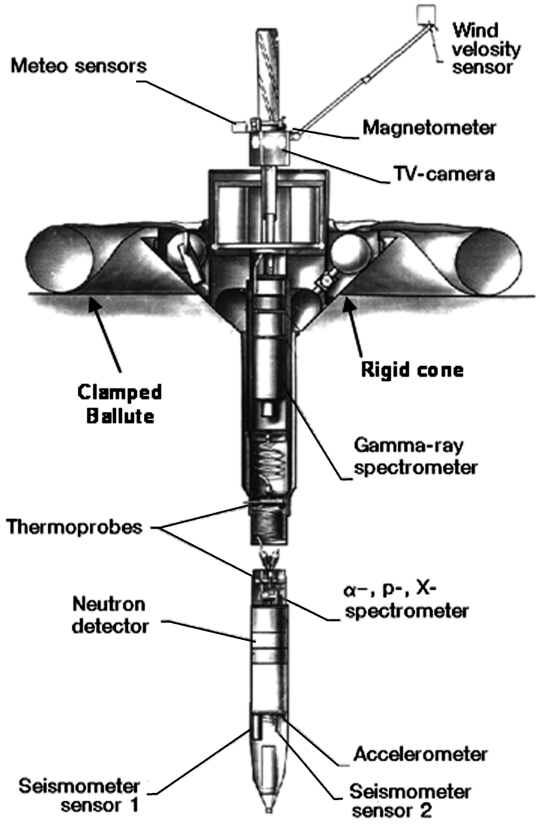

Fig. 21 MARS-96 penetrator schematic showing the rigid cone and clamped ballute [§].

reduction are suggested when possible. This computational aeroelasticity technique was recently demonstrated for a generic launch vehicle in hypersonic flight [71].

Coupled CSD and CFD codes represent a significant advance in modeling of inflatable decelerators, but still lack the ability to find solutions for aerocapture trajectories where flight conditions are in the transitional and free-molecular regimes, and when real-gas effects are important. Many challenges to ballute aeroelastic analysis have been identified and a plan is proposed to overcome them. Ongoing work in this area is described further in Sec. VII of this paper. The complete simulation package would also include coupling to thermal and trajectory analyses so that performance and integrity of the complete system could be evaluated in a fully coupled manner.

VI. FLIGHT TESTING

At the time of this writing (December 2005) no ballute has successfully been flight tested in aerocapture relevant conditions. Successful ballute tests have been achieved for subsonic and supersonic applications [72–75]. Three attempts have been made in Russia and Europe to fly an inflatable decelerator. The first flight model of an inflatable decelerator was on the penetrators for the MARS-96 mission, which failed to leave Earth orbit. The second two attempts were the inflatable reentry descent technology (IRDT) demonstrators. Though the MARS-96 mission and IRDT missions are entry missions, they encounter similar flight conditions as an aerocapture mission.

A. MARS-96 Penetrators

The MARS-96 mission carried two penetrators with surface science and seismology payloads. The penetrator configuration consisted of a long spike with a small rigid cone and an inflatable brake[§]. Figure 21 shows the penetrator layout with the rigid and inflatable brakes identified. The penetrators were to be released during Mars approach and intersect the atmosphere at 5.6 km/s and -12 ± 2 deg flight path angle. Each penetrator had a mass of 45 kg and carried a 4.5 kg scientific payload. Decelerator size was designed to achieve ground impact at 80 ± 20 m/s, resulting in ground penetration up to 6 m. The inflatable brake was a second-stage decelerator designed to deploy at Mach 15 during the Mars atmospheric entry. Unfortunately, on 16 November 1996, the MARS-96 upper stage failed to ignite and the spacecraft reentered the Earth's atmosphere, terminating the mission.

B. Inflatable Reentry Descent Technology

Because of the upper-stage failure of the MARS-96 penetrator mission, an Earth test was proposed for this ballute technology. The test flight planned the return of an instrumented payload from Earth orbit using a two-stage conical ballute. The mission and vehicle parameters are given in [76,77]. The layout and critical dimension of the vehicle are shown in Fig. 22. The aerodynamic decelerator mission profile begins with inflation of the first-stage ballute while still attached to the Fregat upper stage. Separation is commanded and the IRDT ballute encounters the Earth's atmosphere at 100 km altitude, 5.4 km/s, and −7.3 deg flight path angle. The second-stage ballute is deployed at about 30 km altitude and increases the ballistic coefficient by a factor of 5, allowing a slow final descent and impact at 14 m/s. Table 5 lists the planned critical events during entry.

The IRDT test flight took place in February of 2000 aboard a Soyuz/Fregat launch vehicle. Gräßlin and Schöttle [77] describe the postflight recovery and trajectory reconstruction efforts. Upon recovery of the vehicle, inspection revealed destroyed first- and second-stage ballutes, higher than expected ablation of the TPS, full second-stage gas bottles, and an impact-damaged payload canister. Despite the loss of the inflatables and damage to the payload canister,

[§]Data available on-line at http://www.iki.rssi.ru/mars96/09_mars_e.htm [cited June 13, 2005].

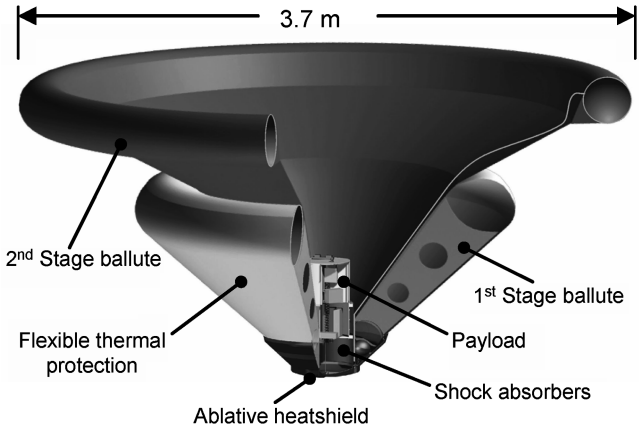

Fig. 22 IRDT configuration [77].

the instruments recorded the flight data and this data was successfully retrieved. Linear acceleration, angular acceleration, pressure, and temperature measurements were recorded. Data recording was started at 150 km altitude, before the 100 km atmospheric interface. Several spikes in the acceleration curve were noted shortly after the start of recording. These spikes are indicative of impact with a foreign object, most likely the payload adapter of the upper stage that induced a tumbling motion, later damped by aerodynamic forces. Upon entry, forces were primarily in the axial direction, indicating proper functioning of the ballute, but about 50 s after entry interface (near peak deceleration) the capsule began to tumble again. The tumbling motion exposed the back of the payload where the pressure sensor is mounted, and increased pressure is observed in the readings corresponding to this region of the trajectory. After about 90 s, the tumbling motion was damped and the vehicle descended at about 60 m/s, significantly above the nominal rate of 14 m/s. The increased descent rate correlates well with the drag produced by the rigid core of the vehicle alone, indicating failure of both ballute stages. A definitive cause of failure was not determined. The Fregat upper stage was also outfitted with a scaled-up version of the IRDT ballute. The Fregat stage entered, but was not recovered.

Because the initial IRDT flight was largely unsuccessful a reflight was planned (IRDT-2). Wilde and Walther [78] describe the improvements to the heatshield design, pressure control system, data acquisition, and telemetry system. Improvements were based on the desire for more complete information in the case of a failure. The packaged layout for IRDT-2 is shown in Fig. 23. The system has a mass of 140 kg, 30 kg more than IRDT due to the extra instrumentation. This flight was initiated on a Russian Volna submarine-launched rocket, and would simulate a 7.8 km/s entry, −2.0 deg flight path angle. Launch occurred on 7 July 2001 but the payload failed to separate from the launch vehicle and the vehicle was never found. An identical reflight named IRDT-2R was launched in October 2005, but has yet to be recovered.

Table 4 Measured and calculated stagnation point results for moderate enthalpy flow in N_2 [59]

Shot	Re_e	Exp. heat rate, ± 3 MW/m^2	Exp. St_e, $\pm 0.7 \times 10^{-3}$	Theory heat rate, MW/m^2	Theory St_e
C1	2090	24	10×10^{-3}	24	10.1×10^{-3}
C2	2800	27	9.3×10^{-3}	26.3	9.06×10^{-3}
C3	2800	25	8.6×10^{-3}	26.3	9.06×10^{-3}
C4	2800	19	6.5×10^{-3}	26.3	9.06×10^{-3}

Table 5 Critical events during entry for IRDT

Entry event	Value	Altitude
Deorbit burn	——	600 km
First-stage deploy	——	200 km
Separation from LV	$T = 0$ s	150 km
Entry interface	5.4 km/s, −7.3 deg	100 km
Peak heat rate	31.3 W/cm^2	61 km
Peak acceleration	13.5 g_E	53 km
Second-stage deploy	——	30 km
Group impact	——	0 km

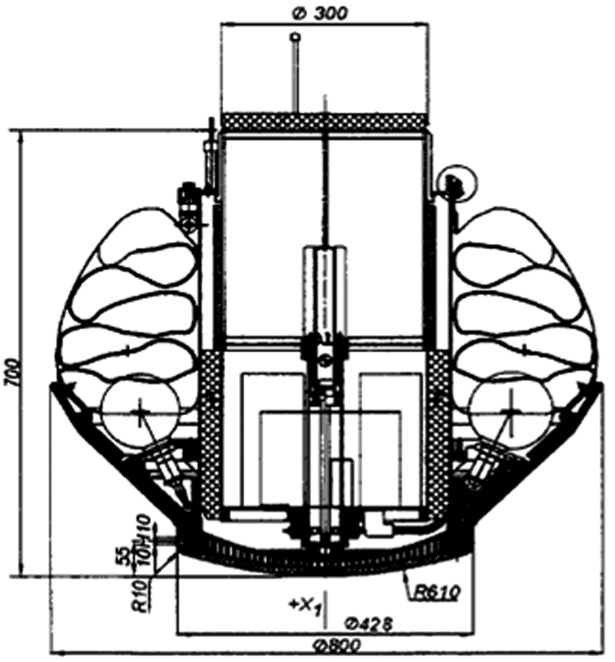

Fig. 23 Packaging layout for IRDT-2 [78].

VII. ADVANCING BALLUTE TECHNOLOGY

Numerous studies have shown the mass advantage of using ballutes for aerocapture and entry. Recent advances in materials technology and integrated aerothermal-structural analysis have spurred a new round of research to develop the concept further. Ongoing work is critically focused on advancing the technology readiness of fabric and thin-film ballute concepts, leading to flight validation.

The inflatable reentry vehicle experiment (IRVE) is currently being developed at NASA Langley Research Center. A clamped fabric ballute composed of concentric toroids is being designed for launch on a sounding rocket [79]. While not entering from orbit, the resulting trajectory will approximate the heating and loads encountered during Earth entry. Figure 24 shows a schematic of the layout of the IRVE vehicle. Launch has been pushed back to late 2006.

The second young engineers' satellite project is a completely student-built project started in 2002. Kruijff et al. [80] describe the mission, detailing the use of a tether to deorbit and "an inherently safe reentry" (AIR) capsule for entry and landing in mainland Europe. AIR is considered inherently safe because it is designed to burn up in

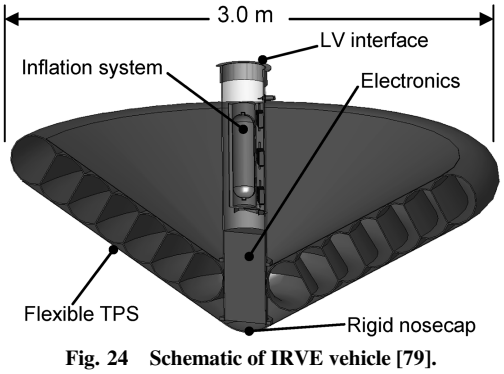

Fig. 24 Schematic of IRVE vehicle [79].

the upper atmosphere if inflation does not occur, and if it works properly the descent speed will be extremely low. The final configuration is to have a mass between 5 and 10 kg and have a terminal velocity of about 7 m/s. Kruijff et al. [81] outline the evolution of the AIR design from a simple inflatable sphere to the inflated sphere-cone specified for the mission. Details and performance of the final configuration are provided in [82].

Numerous systems studies and tool development programs are supporting development of ballutes for aerocapture and entry. A majority of the ballute work in progress is sponsored either through NASA's In-Space Propulsion (ISP) [83] or Exploration Systems Research and Technology (ESR&T) programs. A representative set of this technology development work is described here.

The ongoing ISP work is focused on a comparison of thin-film ballute aerocapture to rigid aeroshell aerocapture at Titan and Neptune for a 500 kg science payload. Current results are summarized in [43] and show that the payload mass fraction is significantly improved using thin-film ballutes. The mission profile uses ballute release to control the exit conditions. The conceptual design study includes aerothermal, packaging, structural, and trajectory analysis and has found no showstoppers. Limited wind tunnel testing has been performed on simplified models to verify analyses. Future work includes aeroelastic analysis, incorporation of tether aerodynamics, and wind tunnel testing of inflated models.

Ballute research sponsored by the NASA ESR&T program focuses on International Space Station down-mass, Earth return from the Moon, and abort options for the crew exploration vehicle. Both direct entry and aerocapture into a low Earth orbit are being considered. These analysis efforts incorporate integrated systems design, aeroelasticity, and materials evaluation. Wind tunnel testing in support of the analytic effort is also planned.

With sufficient investment, the fidelity and accuracy of integrated analysis capabilities will continue to advance. Current capability includes static aeroelastic analysis. CFD codes for entry and aerocapture applications with moving boundaries are being developed, and dynamic aeroelastic solutions along with flutter solutions will be available within five years in all flight regimes. If the current level of technology investment continues, a successful flight test of a clamped ballute will occur in the next five years. Under these same assumptions, the requisite analysis and hypersonic ground-based testing for a thin-film trailing ballute will also be completed within five years, paving the way for flight test of this technology.

VIII. SUMMARY

The concept of the ballute was first theorized in the early 1960s. In the late 1970s and early 1980s, the first ballute aerocapture analyses were completed, identifying a number of technical challenges including the ability to provide lift modulation, sufficient materials thermal-structural characteristics, aerostability, and seam heating. In 1999 and 2000, a resurgence in effort was initiated that continues to the present, in large part due to the concept of the trailing, thin-film ballute. Trailing ballutes offer simple separation but increased mass compared with clamped ballutes with equivalent heat rates. A number of ballute technical challenges have been documented and the aeroassist community is presently focused on their solution. There is significant interest in applying ballute technology at Earth and in other planetary atmospheres. Though detailed studies have not been completed, preliminary analysis indicates feasibility and significant mass savings over propulsive orbit insertion.

The issue of optimal ballute shape is tightly coupled with the flow stability problem and the application. For aerocapture at Titan, a toroidal geometry has been analyzed in all flight regimes and shown to produce steady flow (including the interference effects of the parent spacecraft). Tethers were not included, but separate analysis was conducted to determine the heat rate on the tethers and insulation was added as necessary. Material testing of thin-film polymers has indicated adequate strength at temperature to survive the drag forces with minimal reinforcements at the tether attach points. Mechanical tests of seaming techniques are underway. Parent spacecraft protection was addressed through modeling and it was determined that insulation blankets would be sufficient to protect the spacecraft from the heating environment encountered. Trajectory work and ballute release algorithm development have indicated that ballute aerocapture at Titan is feasible when uncertainties are accounted for. Minimal wind tunnel testing has been performed to date, with the limited tests conducted being aimed at validation of computational methods. Challenges still exist for the Titan aerocapture mission, specifically aeroelastic analysis, deployment, thin-film seaming, radiative heating, and experimental verification.

Efforts are currently underway to develop the tools necessary for aeroelastic analysis. Once developed, these tools will require experimental validation. Deployment techniques for large pressure stabilized structures can be advanced from efforts in solar sails and inflatable antennas, but specific implementation options require adaptation to ballute geometries.

Determination of radiative heating is a major outstanding issue, particularly in the transitional aerodynamic regime. In the 1980s theories were developed that agreed with data from flight test at Earth with reasonable accuracy, but were not known to be valid at the altitudes where ballutes decelerate. Furthermore, limited data is available to validate gasdynamic models for other planetary atmospheres.

Advancement of thin-film ballute technology to the flight-test stage looks promising with additional technology development in the areas of integrated analysis, high temperature materials and their seaming, and hypersonic testing. Flight test of a clamped fabric ballute appears likely within the next five years. With completion of a ballute flight-test program, incorporation of ballute technology as part of a planetary exploration mission may soon become a viable option.

References

[1] Warzecha, L. W., "Performance and Design Considerations for Maneuvering Space Vehicles," IAS Paper 60-59, June–July 1960.

[2] London, H. S., "Change of Satellite Orbit Plane by Aerodynamic Maneuvering," *Journal of the Aerospace Sciences*, Vol. 29, No. 3, 1962, pp. 323–332.

[3] Kayser, L. D., "Pressure Distribution, Heat Transfer, and Drag Tests on the Goodyear Ballute," AEDC TDR-62-39, March 1962.

[4] Walberg, G. D., "A Survey of Aeroassisted Orbit Transfer," *Journal of Spacecraft and Rockets*, Vol. 22, No. 1, 1985, pp. 3–18.

[5] Hall, J. L., and Le, A. K., "Aerocapture Trajectories for Spacecraft with Large, Towed Ballutes," *Advances in the Astronautical Sciences*, Vol. 108 II, Univelt, San Diego, CA, 2001, pp. 1857–1872.

[6] Hall, J. L., Noca, M. A., and Bailey, R. W., "Cost-Benefit Analysis of the Aerocapture Mission Set," *Journal of Spacecraft and Rockets*, Vol. 42, No. 2, 2005, pp. 309–320.

[7] Maynard, J. D., "Aerodynamic Characteristics of Parachutes at Mach Numbers from 1.6 to 3," NASA TN-D-752, May 1961.

[8] McShera, J. T., Jr., and Keyes, J. W., "Wind-Tunnel Investigation of a Balloon as a Towed Decelerator at Mach Numbers from 1.47 to 2.50," NASA TN-D-919, Aug. 1961.

[9] Charczenko, N., and McShera, J. T., Jr., "Aerodynamic Characteristics of Towed Cones Used as Decelerators at Mach Numbers from 1.57 to 4.65," NASA TN-D-994, Dec. 1961.

[10] McShera, J. T., Jr., "Aerodynamic Drag and Stability Characteristics of Towed Inflatable Decelerators at Supersonic Speeds," NASA TN-D-1601, Mar. 1963.

[11] Couch, L. N., "Drag and Stability Characteristics of a Variety of Reefed and Unreefed Parachute Configurations at Mach 1.80 with an Empirical Correlation for Supersonic Mach Numbers," NASA TR-R-429, Feb. 1975.

[12] Alexander, W. C., "A Discussion of Governing Decelerator Performance and Design Parameters in the Supersonic Flight Regime," AIAA Paper 68-938, Sept. 1968.

[13] Alexander, W. C., and Lau, R. A., "State-of-the-Art Study for High-Speed Deceleration and Stabilization Devices," NASA CR-66141, Sept. 1966.

[14] Musil, J. L., "Study of Expandable, Terminal Decelerators for Mars Atmosphere Entry," Goodyear Aerospace Corp., Rept. GER-12842, Vol. 1, Akron, OH, 21 Oct. 1966.

[15] McShera, J. T., Jr., and Bohon, H. L., "A Summary of Supersonic Decelerators with Emphasis on Problem Areas in Aerodynamics and Structures," AIAA Paper 67-201, Jan. 1967.

[16] Guy, L. D., "Structural and Decelerator Design Options for Mars Entry," *Journal of Spacecraft and Rockets*, Vol. 6, No. 1, 1969, pp. 44–49.
[17] Gillis, C. L., "Deployable Aerodynamic Decelerators for Space Missions," *Journal of Spacecraft and Rockets*, Vol. 6, No. 8, 1969, pp. 885–890.
[18] Andrews, D. G., and Bloetscher, F., "Aerobraked Orbital Transfer Vehicle Definition," AIAA Paper 81-0279, Jan. 1981.
[19] Grenich, A. F., and Woods, W. C., "Flow Field Investigation of Atmospheric Braking for High Drag Vehicles with Forward Facing Jets in Spacecraft Entry," AIAA Paper 81-0293, Jan. 1981.
[20] Heitchue, R. D., "Emergency Space Station Escape System Consisting of Retrorocket, Expandable Reentry Structure, Life Support Unit, Survival Provisions and Communications Beacons," *Advances in the Astronautical Sciences*, edited by N. V. Peterson, Vol. 16, No. 1, AAS Space Rendezvous, Rescue, and Recovery, Western Periodicals, North Hollywood, CA, 1963, pp. 680–692.
[21] Kendall, R. T., "Techniques for Space and Hypersonic Flight Escape," *Proceedings of SAE Aerospace Systems Conference*, Society of Automotive Engineers, New York, 1967, pp. 394–400.
[22] Kendall, R. T., Jr., and Kendall, R. T., Sr., "Advanced Unmanned/Manned Space Payload Inflatable Decelerator/Delivery System," AIAA Paper 95-3798, Sept. 1995.
[23] Kendall, R. T., and Maddox, A. R., "The Use of Inflatable Structures for Re-entry of Orbiting Vehicles," SAE Paper 901835, Oct. 1990.
[24] Cruz, M. I., "The Aerocapture Vehicle Mission Design Concept," AIAA Paper 79-0893, May 1979.
[25] Wercinski, P. F., Henline, W., Tran, H., Milos, F., Papadopoulos, P., Chen, Y. K., Venkatapathy, E., and Tauber, M., "Trajectory, Aerothermal Conditions, and Thermal Protection System Mass for the Mars 2001 Aerocapture Mission," AIAA Paper 97-0472, Jan. 1997.
[26] French, J. R., and Cruz, M. I., "Aerobraking and Aerocapture for Planetary Missions," *Astronautics and Aeronautics*, Vol. 18, No. 2, 1980, pp. 48–55, 71.
[27] Braun, R. D., and Powell, R. W. "Aerodynamic Requirements of a Manned Mars Aerobraking Transfer Vehicle," *Journal of Spacecraft and Rockets*, Vol. 28, No. 4, 1991, pp. 361–367.
[28] Braun, R. D., Powell, R. W., and Lyne, J. E., "Earth Aerobraking Strategies for Manned Return from Mars," *Journal of Spacecraft and Rockets*, Vol. 29, No. 3, 1992, pp. 297–304.
[29] Powell, R. W., and Braun, R. D., "A Six Degree-of-Freedom Guidance and Control Analysis of Mars Aerocapture," *Journal of Guidance, Control, and Dynamics*, Vol. 16, No. 6, 1993, pp. 1038–1044.
[30] Mulqueen, J. A., "Applications of Low Lift to Drag Ratio Aerobrakes Using Angle of Attack Variation for Control," NASA TM-103544, June 1991.
[31] Jits, R. Y., and Walberg, G. D., "High L/D Mars Aerocapture for 2001, 2003, and 2005 Mission Opportunities," AIAA Paper 1998-0299, Jan. 1998.
[32] Ling, L., Baseggio, F. M., and Fuhry, D. P., "Parametric Entry Corridors for Lunar/Mars Aerocapture Missions," NASA TM-102178, April 1991.
[33] Kustas, F. M., Rawal, S. P., Willcockson, W. H., Edquist, C. T., Thornton, J. M., and Sandy, C., "Inflatable Decelerator Ballute for Planetary Exploration Spacecraft," AIAA Paper 2000-1795, Apr. 2000.
[34] Kustas, F. M., Rawal, S. P., Willcockson, W. H., Edquist, C. T., Thornton, J. M., and Giellis, R. T., "Attached Inflatable Ballute for Spacecraft Deceleration," *Proceedings of the IEEE Aerospace Conference*, Vol. 7, Institute of Electrical and Electronics Engineers, Piscataway, NJ, 2000, pp. 421–427.
[35] McRonald, A. D., "A Light-Weight Inflatable Hypersonic Drag Device for Planetary Entry," AIAA Paper 99-0422, Mar. 1999.
[36] Cruz, J. R., Cianciolo, A. D., Powell, R. W., Simonsen, L. C., and Tolson, R. H., "Entry, Descent, and Landing Technology Concept Trade Study for Increasing Payload Mass to the Surface of Mars," Atmospheric Reentry Association, Mar. 2005.
[37] Yavrouian, A., Yen, S. P. S., Plett, G., and Weissman, N., "High Temperature Materials for Venus Balloon Envelopes," AIAA Paper 95-1617, May 1995.
[38] Yavrouian, A., Plett, G., Yen, S. P. S., Cutts, J., and Baek, D., "Evaluation of Materials for Venus Aerobot Applications," AIAA Paper 99-3859, June–July 1999.
[39] McRonald, A. D., "A Light-Weight Inflatable Hypersonic Drag Device for Venus Entry," AAS Paper 99-355, Aug. 1999.
[40] McRonald, A. D., "A Light-Weight Inflatable Hypersonic Drag Device for Neptune Entry," AIAA Paper 2000-123, Jan. 2000.
[41] Hall, J., L., "A Review of Ballute Technology for Planetary Aerocapture," AIAA Paper 2000-382, May 2000.
[42] Freeland, R. E., Bilyeu, G. D., Veal, G. R., Steiner, M. D., and Carson, D. E., "Large Inflatable Deployable Antenna Flight Experiment Results," *Acta Astronautica*, Vol. 41, Nos. 4–10, 1997, pp. 267–277.
[43] Miller, K. L., Gulick, D., Lewis, J., Lyons, D., Stein, J., and Wilmoth, R., "Trailing Ballute Aerocapture: Concept and Feasibility Assessment," AIAA Paper 2003-4655, July 2003.
[44] Westhelle, C. H., and Masciarelli, J. P., "Assessment of Aerocapture Flight at Titan Using a Drag-Only Device," AIAA Paper 2003-5389, Aug. 2003.
[45] Johnson, W. R., and Lyons, D. T., "Titan Ballute Aerocapture Using a Perturbed TitanGRAM Model," AIAA Paper 2003-5280, Aug. 2003.
[46] Lyons, D. T., and Johnson, W. R., "Ballute Aerocapture Trajectories at Neptune," AIAA Paper 2004-5181, Aug. 2004.
[47] Houtz, N. E., "Optimization of Inflatable Drag Devices by Isotensoid Design," AIAA Paper 64-437, June–July 1964.
[48] Anderson, R. A., "Structures Technology—1964," *Astronautics and Aeronautics*, Vol. 2, No. 12, 1964, pp. 14–20.
[49] Anderson, M. S., Robinson, J. C., Bush, H. G., and Fralich, R. W., "A Tension Shell Structure for Application to Entry Vehicles," NASA TN-D-2675, Mar. 1965.
[50] Weeks, G. E., "Buckling of a Pressurized Toroidal Ring Under Uniform External Loading," NASA TN-D-4124, Aug. 1967.
[51] Kyser, A. C., "Deployment Mechanics for an Inflatable Tension-Cone Decelerator," NASA CR-929, Nov. 1967.
[52] Prada y Nogueira, I. A., Forlivesi, F., and Morel, Q., "The FEM Applicability for the First-Stage Design of Inflatable Bodies. Iterative Methodology Between FD and FEM for the Inherently Safe Re-Entry Capsule for YES2. The Breogan Leakage Protection System," IAC Paper 03-U.3.04, Sept.–Oct. 2003.
[53] Wang, J. T., Chen, T., Sleight, D. W., and Tessler, A., "Simulating Nonlinear Deformations of Solar Sail Membranes Using Explicit Time Integration," AIAA Paper 2004-1580, Apr. 2005.
[54] Tessler, A., Sleight, D. W., and Wang, J. T., "Nonlinear Shell Modeling of Thin Membranes with Emphasis on Structural Wrinkling," AIAA Paper 2003-1931, Apr. 2003.
[55] Su, X., Abdi, F., Taleghani, B., and Blandino, J. R., "Wrinkling Analysis of a Kapton Square Membrane Under Tensile Loading," AIAA Paper 2003-1985, Apr. 2003.
[56] Gnoffo, P. A., "Planetary-Entry Gas Dynamics," *Annual Review of Fluid Mechanics*, Vol. 31, Jan. 1999, pp. 459–494.
[57] Rasheed, A., Fujii, K., Hornung, H. G., and Hall, J. L. "Experimental Investigation of the Flow Over a Toroidal Aerocapture Ballute," AIAA Paper 2001-2460, June 2001.
[58] Hornung, H. G., "Hypersonic Flow Over Bodies in Tandem," *Shock Waves*, Vol. 11, No. 6, 2002, pp. 441–445.
[59] McIntyre, T. J., Lourel, I., Eichmann, T. N., Morgan, R. G., Jacobs, P. A., and Bishop, A. I., "Experimental Expansion Tube Study of the Flow Over a Toroidal Ballute," *Journal of Spacecraft and Rockets*, Vol. 41, No. 5, 2004, pp. 716–725.
[60] Gnoffo, P. A., "An Upwind-Biased, Point-Implicit Relaxation Algorithm for Viscous Compressible Perfect Gas Flows," NASA TP-2953, Feb. 1990.
[61] Gnoffo, P. A., "Computational Aerothermodynamics in Aeroassist Applications," *Journal of Spacecraft and Rockets*, Vol. 40, No. 3, 2003, pp. 305–312.
[62] Gnoffo, P. A., Gupta, R. N., and Shinn, J. L., "Conservation Equations and Physical Models for Hypersonic Air Flows in Thermal and Chemical Nonequilibrium," NASA TP-2867, 1989.
[63] Gnoffo, P. A., and Anderson, B. P., "Computational Analysis of Towed Ballute Interactions," AIAA Paper 2002-2997, June 2002.
[64] Anderson, B. P., "Computational Continuum and Rarefied Flow Results for Ballute Applications," AIAA Paper 2004-292, Jan. 2004.
[65] Park, C., "A Survey of Aerobraking Orbital Transfer Vehicle Design Concepts," AIAA Paper 87-514, Jan. 1987.
[66] Park, C., "Theory of Idealized Two-Dimensional Ballute in Newtonian Hypersonic Flow," *Journal of Spacecraft and Rockets*, Vol. 25, No. 3, 1988, pp. 217–224; also AIAA Paper 86-301.
[67] Abe, T., "A Self-Consistent Tension Shell Structure for Application to Aerobraking Vehicle and Its Aerodynamic Characteristics," AIAA Paper 88-3405, July 1988.
[68] Mosseev, Y., "The Multipurpose Integrated PC-Software for Structural and Aeroelastic Analysis of Decelerators, Paragliders and Balloons," AIAA Paper 97-1455, June 1997.
[69] Mosseev, Y., "The Decelerator Pitch-Dependent Performances Prediction Based on 3D Aeroelastic Analysis," AIAA Paper 99-1717, June 1999.
[70] Bartels, R. E., Moses, R. W., Scott, R. C., Templeton, J. D., Cheatwood, F. M., Gnoffo, P. A., and Buck, G. M., "A Proposed Role of

Aeroelasticity in NASA's New Exploration Vision," DGLR Paper IF-013, June–July 2005.
[71] Thuruthimattam, B. J., Friedmann, P. P., McNamara, J. J., and Powell, K. G., "Aeroelasticity of a Generic Hypersonic Vehicle," AIAA Paper 2002-1209, Apr. 2002.
[72] Graham, J. J., Jr., "Development of Ballute for Retardation of Arcas Rocketsondes," AFCRL 65-877, Dec. 1965.
[73] Mayhue, R. J., and Eckstrom, C. V., "Flight-Test Results from Supersonic Deployment of an 18-Foot-Diameter (5.49-Meter) Towed Ballute Decelerator," NASA TM-X-1773, May 1969.
[74] White, W. E., and Riddle, C. D., "An Investigation of the Deployment Characteristics and Drag Effectiveness of the Gemini Personnel Decelerator at Subsonic and Supersonic Speeds, Phase II," AEDC TDR-63-255, Dec. 1963.
[75] Smith, T. R., Shook, L., Uhelsky, F., McCoy, E., , Krasinski, M., and Limaye, S., "Ballute and Parachute Decelerators for FASM/QuickLook UAV," AIAA Paper 2003-2142, May 2003.
[76] Ivanov, S. V., Koulikov, S.D., Pichkhadze, K. M., Serdyuk, V. K., Kassing, D., Marraffa, L., and Wilde, D., "New Technology of Payload Return from Space to the Earth," IAF Paper IAF-00-V.2.04, Oct. 2000.
[77] Gräßlin, M., and Schöttle, U., "Flight Performance Evaluation of the Re-Entry Mission IRDT-1," IAF Paper IAF-01-V.3.05, Oct. 2001.
[78] Wilde, D., and Walther, S., "Flight Test and ISS Application of the Inflatable Reentry and Descent Technology (IRDT)," *Acta Astronautica*, Vol. 51, No. 1–9, 2002, pp. 83–88.
[79] Hughes, S. J., Dillman, R.A., Starr, B. R., Stephan, R. A., Lindell, M. C., Player, C. J., and Cheatwood, F. M., "Inflatable Re-Entry Vehicle Experiment (IRVE) Design Overview," AIAA Paper 2005-1636, May 2005.
[80] Kruijff, M., Van der Heide, E. J., and Calzada Gil, S., "YES2 Inherently-Safe Tethered Re-Entry Mission and Contingencies," IAC Paper IAC-03-IAA.6.2.02, Sept.–Oct. 2003.
[81] Kruijff, M., Van der Heide, E. J., Dragoni, E., Castagnetti, D., and Ferretti, S., "Concept Selection and Design of the Inherently Safe Re-Entry Capsule for YES2," IAC Paper IAC-03-V.3.08, Sept.–Oct. 2003.
[82] Morel, Q., Hobbs, S., and Kruijff, M., "Cranfield's Inherently Safe Re-Entry Capsule Design for YES2," IAC Paper IAC-03-U.1.07, Sept.–Oct. 2003.
[83] James, B., Munk, M., and Moon, S., "Aerocapture Technology Project Overview," AIAA Paper 2003-4654, July 2003.
[84] Johnson, B. A., "Design, Fabrication, and Static Testing of First-Stage Attached Inflatable Decelerator (AID) Models," NASA CR-111934, 1971.

C. Kluever
Associate Editor